THE JOURNAL OF PHYSICAL CHEMISTRY B

Article

pubs.acs.org/JPCB

Microbubble Formation from Plasma Polymers

Anaram Shahravan, Srinath Yelamarty, and Themis Matsoukas*

Department of Chemical Engineering, The Pennsylvania State University, University Park, Pennsylvania 16802, United States

Supporting Information

ABSTRACT: We document the formation of liquid-like particles in a toluene glow discharge that subsequently solidify via a process that releases hydrogen to form a solid microbubble with micrometer-size diameter, nanometer-size shell thickness, and high volume fraction, in excess of 90%. Liquid-like particles are produced in a toluene plasma under conditions that promote low degree of cross-linking (low power, high pressure). When these are transferred for observation in TEM, they are seen to transform under irradiation by the electron beam into solid bubbles with diameter of about 3 μm. This transformation also takes place under laser irradiation of sufficient power and under heating. We present evidence that the formation of these microbubbles is due to solidification of the liquid-like precursor that is accompanied by release of hydrogen. This mechanism is supported by a geometric model that provides a quantitative description of the particle size before and after solidification. These unique stimuli-responsive particles exhibit the potential of using temperature, electron beam, or laser as a source to change their size and structure which may find application in thermal insulators, lightweight materials, and light scattering agents.

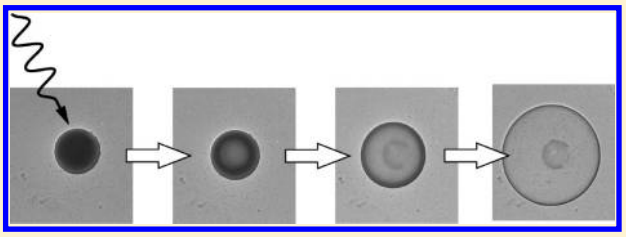

INTRODUCTION

Hollow micro-/nanospheres are materials that provide a means for storage, insulation, and fabrication of low density devices and foams.[1−3] They are potentially useful as encapsulation vehicles for drugs, cosmetics, gene, DNA, and enzyme,[4−7] as catalytically active materials and as acoustical and thermal insulators.[8−10] Because of their distinctive scattering and adsorption properties, they have been used in pigment and paper coating applications.[11,12] Hollow nanoparticles are prepared either through a template-assisted or through a template-free method. In the template-assisted process, a core particle (template) is coated with the shell material, and the template is then removed chemically or by thermal decomposition.[13] The template-assisted method has been used for large-scale fabrication and for synthesis of hollow particles with different sizes and shapes. In the template-free method, the hollow particle is produced in a single step through various mechanisms, including flame pyrolysis of liquid droplets,[14,15] liquid-to-solid conversion,[16−19] and crystal dissolution equilibria.[20] The template-free method is more challenging because it is not easily generalized from one material to another, but it presents the significant advantage that it does not require the additional processing steps involved in template-assisted processing.

Several inorganic materials have been made into hollow spheres in a one-step process involving an inside-out evacuation procedure, which has been explained by a dissolution−recrystallization mechanism that was first described by Wilhelm Ostwald.[21,20] Hollow structures can also be formed by exposure of particles to temperature, pressure, and pH shifts and by absorption of energy in the form of electric and magnetic fields and light,[22−25] and in some cases under the irradiation of an electron beam when the sample is studied in TEM.[26,27] These examples highlight the variety of mechanisms by which homogeneous particles may be transformed into core−shell nanostructures.

Conventional polymeric materials have been observed to produce hollow nanoparticles by the one-step process.[28] Plasma polymers (PP) are nonconventional solids that can form nanoparticles as well as hollow nanospheres.[16,29,30] Over the past 60 years plasma polymerization has been used to coat substrates with thin films[31−33] for applications in biological, pharmaceutical, and electrical systems.[34−37] Plasma polymerization mostly occurs in low-pressure electrical discharges when organic gases and vapors, such as methane, isopropanol, parylene, toluene, and etc., are delivered to the plasma.[38,39] The gas discharge produces reactive species from the original gas or vapor monomer, and the final product is typically a solid material that consists of a cross-linked network of amorphous hydrogenated carbon. These materials are chemically inert and exhibit low friction and low dielectric constant.[40,41] Though mainly plasma polymers are deposited as films, it is also possible to produce nanoparticles via gas-phase nucleation.[42−44] Particles by plasma polymerization have been used for plastic and rubber products, nanofluids, and controlled release applications because of the controllability over their size, hydrophobic properties, and their mechanical properties.[45,46] The degree of cross-linking depends on the operating parameters of the plasma; however, generally, high power and low pressure promote the formation of solid materials with a high degree of cross-linking, whereas low power and higher pressure promote the formation of viscous oily liquids.[47,48] In

Received: April 19, 2012
Revised: August 19, 2012
Published: September 6, 2012

 © 2012 American Chemical Society dx.doi.org/10.1021/jp303793u | J. Phys. Chem. B 2012, 116, 11737−11743

this work, we describe the formation of liquid-like nanoparticles in a toluene plasma that undergo a liquid-to-solid transformation to produce solid microbubbles, namely, micrometer-size spheres that consist of a thin solid shell and a large empty void in the middle. We present material characterizations of the microbubbles, investigate energy sources that can induce the solidification of the bubbles, and present evidence for the proposed mechanism of formation.

EXPERIMENTAL SECTION

Synthesis. Particles are produced in a semibatch tubular pyrex reactor, shown in Figure 1, by plasma polymerization of

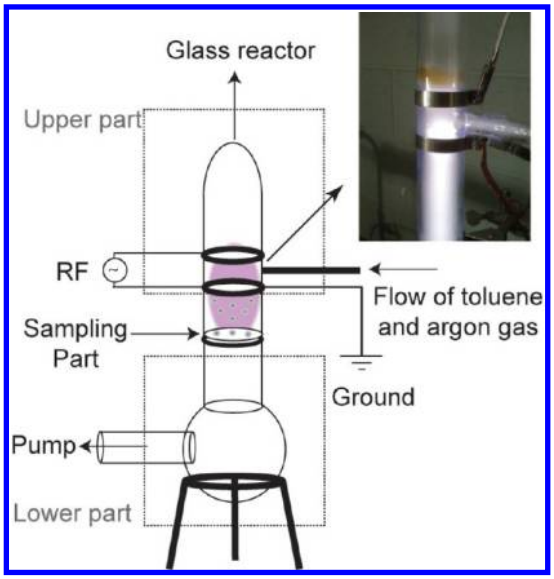

Figure 1. Schematic of the plasma reactor.

toluene at a pressure of 200−400 mTorr. Toluene (99.5% pure) was obtained from J. T. Baker as the feed supply for the reaction. The reactor chamber consists of two parts that are connected with a flange sealed by a metal clamp ring. This connection point provides a port to access the pyrex reactor for the purpose of collecting particles. Toluene vapor and argon gas enter from the top via a 0.25 in. diameter tube. The plasma is generated by two aluminum rings placed outside the glass reactor at a distance of 3 cm from each other. The top ring is connected to the radio frequency (RF) power supply, and the bottom one is grounded. The RF power supply is connected to an automatic matching network and produces a RF signal at 13.56 MHz, whose power is manually controlled from 5 to 20 W. Particles formed in the plasma are collected on the surface of a filter placed at the flange that links the two parts of the reactor. The toluene vapor is delivered to the reactor using a glass bubbler that is connected to the flow of carrier gas (argon). Toluene vapor flow rate is 2 sccm, while the argon flow rate is 12 sccm. The temperature of the bubbler is kept constant in a water bath. The flow rate of argon flow is controlled with a mass flow controller, while the toluene vapor flow rate is controlled by the water bath temperature. The vacuum is produced by a roughing pump equipped with a liquid nitrogen trap. The reactor pressure before delivering argon gas and toluene vapor is 1 mTorr and is increased to a higher pressure of 200 or 400 mTorr, during the experiment. Excess vapor is condensed on the cold surface of the liquid nitrogen trap to prevent pump contamination.

Characterizations. Transmission electron microscopy (TEM) studies were conducted in a Philips 420 instrument. Particles were collected on 200 square mesh copper grids. Videos and transmission electron micrographs were recorded and captured using a digital CCD camera connected to TEM. Fourier transform infrared (FTIR) spectra were obtained in the range from 850 to 4000 cm^{-1} using a Bruker IFS 66/S FT-IR spectrometer.

RESULTS

Particles collected from the plasma appear in TEM as dark spheres (Figure 2(a)), approximately 1 μm in diameter. Almost

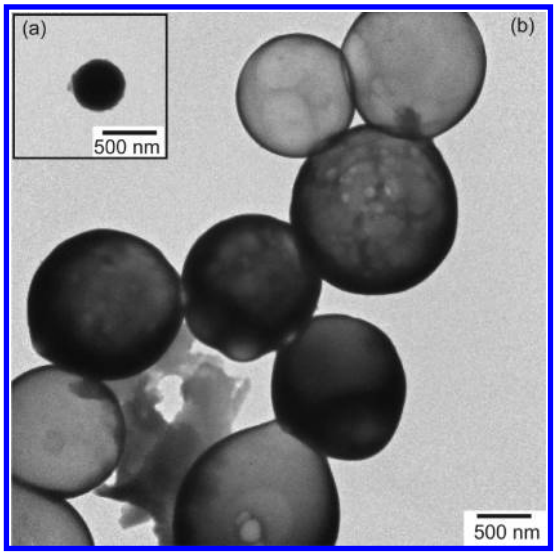

Figure 2. Transmission electron micrographs of (a) a single 480 nm plasma polymerized toluene particle before exposing to an electron beam and (b) the same particles after exposing to an electron beam.

immediately upon focusing the beam, these particles begin to grow and expand until a stable micrometer-sized bubble is formed, with solid walls and a large void, as seen in Figure 2(b). The final particle is a solid bubble, about twice as large as the original particle, with thin walls that appear solid and remain stable under further irradiation by the electron beam. The conversion process has been observed multiple times in real time and was captured by video. (See the video in the Supporting Information.) A series of images extracted from the video (see Figure 3) show the entire process. The first panel (Figure 3(a)) shows the particle 0.6 s after focusing the beam. This particle appears as a dark compact sphere with the highest contrast (darkest point) at the center. At about 1 s (Figure 3(b)), a small void forms at the center of the particle and is recognized by the lighter contrast at the middle. Within the next 10 s, the diameter grows rapidly; the interior of the particle becomes lighter; and the location of the highest contrast moves from the center to the circumference. Within 12 s of focusing the beam, the particle is fully transformed into a micrometer-sized bubble with thin solid walls. A small contraction of size is generally observed right before the bubble reaches its final size (see panels i and j in Figure 3). Figure 4 shows the size of the same particle, plotted as a function of time. The size increases roughly linearly with time and exhibits a small contraction before it settles to its final value. This behavior was observed with all particles on the grid and was reproduced between independent runs of the reactor. Observation under tilted

dx.doi.org/10.1021/jp303793u | J. Phys. Chem. B 2012, 116, 11737−11743

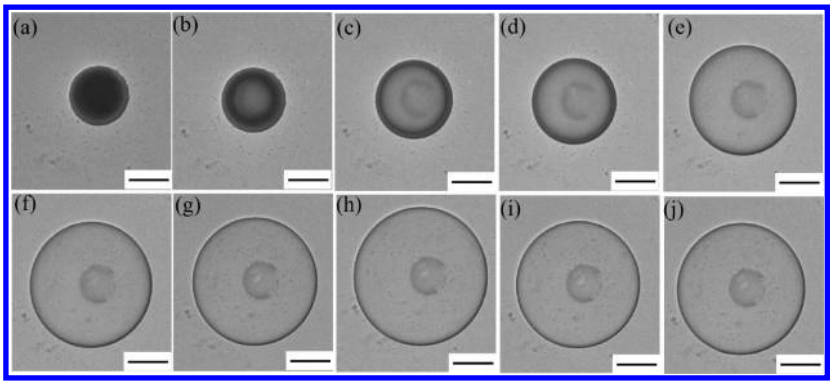

Figure 3. Transmission electron micrographs of a single 3.23 μm toluene plasma polymer at (a) 0.6, (b) 1.05, (c) 1.84, (d) 2.24, (e) 3.62, (f) 4.6, (g) 5.48, (h) 6.33, (i) 7.5, and (j) 12.4 s after exposure to the 120 keV electron beam. Scale bars are 1 μm.

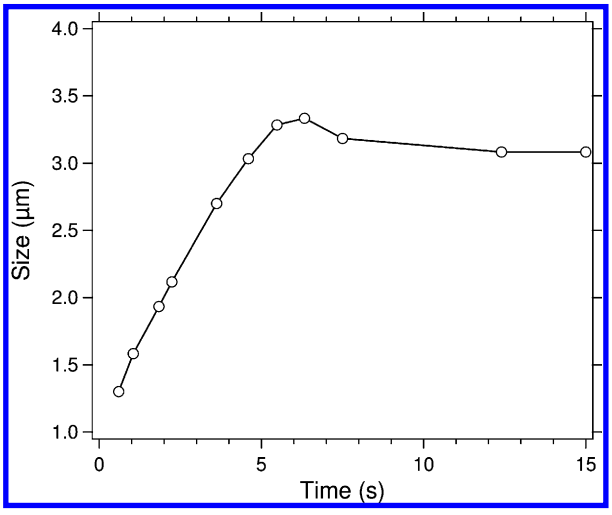

Figure 4. Time evolution of particle size under the influence of TEM.

angles shows that the microbubbles are nearly perfect spheres (Figure 5b and c) except at the contact point (Figure 5d). This image also shows that the small circle that appears to be formed

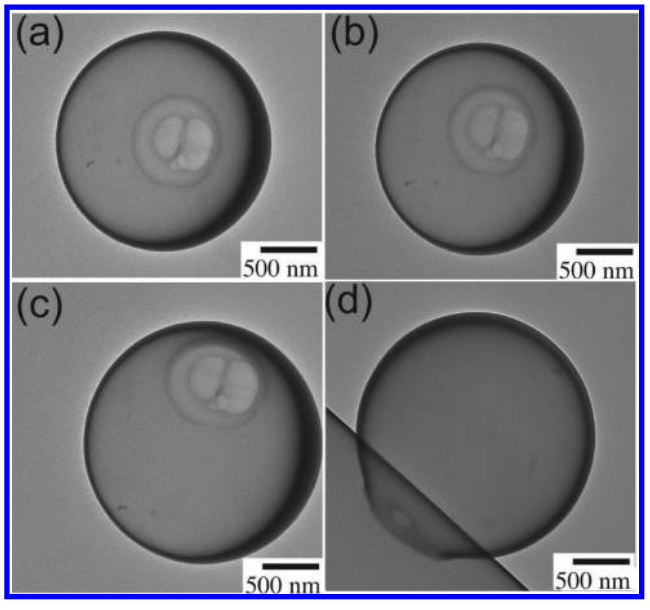

Figure 5. TEM pictures of a single hollow particle at different tilting angles: (a) 0°, (b) 10°, and (c) 30°. (d) Side view.

in the middle of the bubble (see panels c through j in Figure 3) is the contact area between the bubble and the substrate. Hollow spheres have radially uniform shell thicknesses of 47 ± 18 nm and a high void fraction that is 90 ± 3% of the volume of the particle. The size distribution before and after exposure to TEM is shown in Figure 6. The average diameter approximately

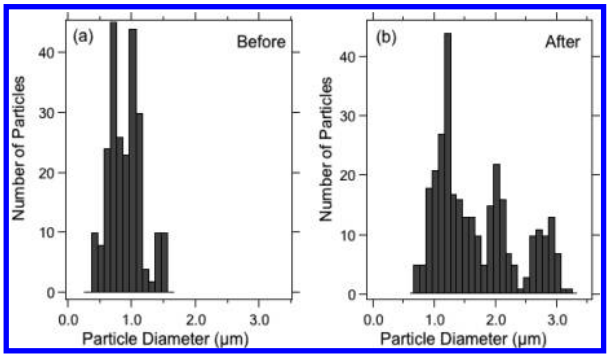

Figure 6. Size distribution for particles before and after exposure to the electron beam.

doubles after exposure to the TEM beam, from an initial size of 0.83 ± 0.26 to 1.60 ± 0.60 μm. These numbers are averages from 320 independent experiments. We note here that heptane under the same conditions was also observed to produce microbubbles. For the remainder of this study, however, we will focus on toluene exclusively.

Particles before and after exposure to TEM were collected, pressed into a KBr pellet, and studied by Fourier transform IR spectroscopy (FTIR). The spectrum of particles before exposure to TEM (Figure 7a) shows a strong adsorption peak at 3050 cm^{-1}, which is characteristic of the aromatic CH stretches, typically present in the 3050−3090 cm^{-1} range.[49] Absorption bands are observed at 2980 and 1660 cm^{-1}, corresponding to sp^3 C−H (alkyl) stretching and the alkene group, C═C, respectively. After exposure to the beam (Figure 7b), the spectrum contains adsorption bands at 2860 and 2930 cm^{-1} that are assigned to alkyl CH stretches. The most important difference is in the aromatic group, which is clearly present before exposure to the electron beam but absent after irradiation. Accordingly, particles formed in the plasma retain a significant degree of the chemical structure of the precursor molecules (toluene), but this is subsequently lost when particles are exposed to the TEM beam. This shows that the beam induces further reaction that completes the transformation of the precursor into the final solid material.

dx.doi.org/10.1021/jp303793u | J. Phys. Chem. B 2012, 116, 11737−11743

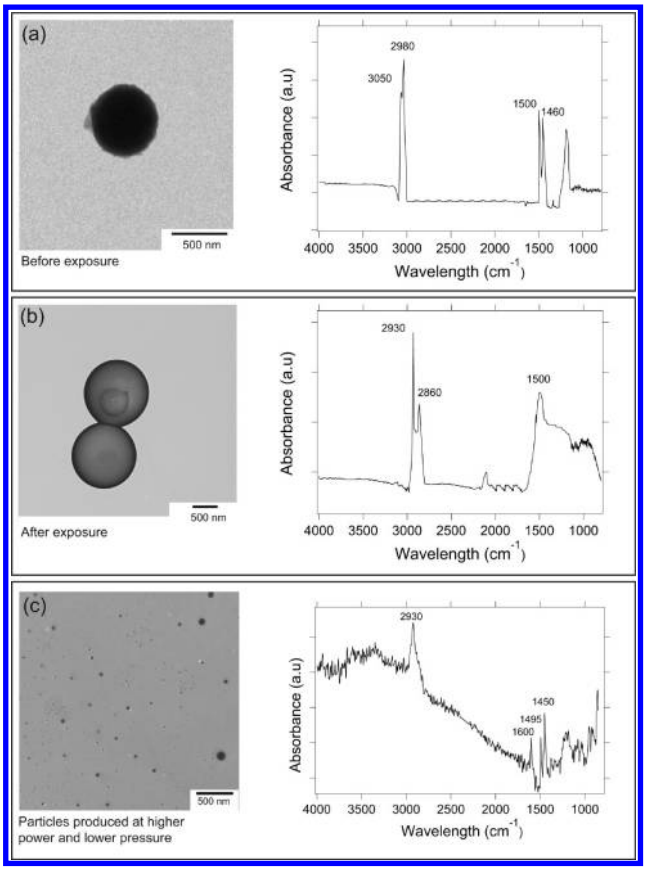

Figure 7. Transmission electron micrographs and FTIR spectrum of plasma polymerized toluene particles (a) before exposure to the electron beam and (b) after exposure to the electron beam and (c) solid particles formed at a RF power of 20 W.

The formation of microbubbles occurs under the action of the electron beam in the TEM, but other forms of energy induce the same transformation. Specifically, we examined the effects of laser irradiation and heating. For the laser experiments, particles were subjected to a pulsed laser beam irradiated from an argon laser (Coherent Innova 300C) for 1 min with two different intensities, 3423.5 and 6847 W/cm^2, while they were suspended in an aqueous solution. Figure 8 shows TEM images of the particles after treatment. The images show the presence of large hollow particles. Though these particles do not have the smooth appearance of those formed under TEM, they are clearly of the same type and consist of a thin shell that surrounds a large empty core. No formation of new bubbles is observed when these particles are examined in TEM, indicating that the transformation was complete under laser irradiation.

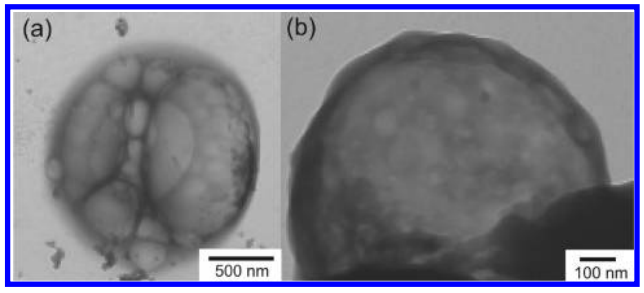

Figure 8. TEM of a toluene-plasma particle exposed to an (a) argon-ion laser working at 100 mW and (b) an argon-ion laser working at 200 mW.

Heating provides yet another means of converting the plasma particles into hollow spheres and offers additional control of the process via temperature. For this experiment, four samples of particles collected from the plasma were subjected to heating in a furnace (thermolyne model FB1400) at constant temperature (100, 200, 250, and 300 °C) for 5 min. Their TEM images in Figure 9 indicate that hollow particles begin to form at a temperature as low as 100 °C. Particles heated to 200 and 250 °C show a collapse of structure into a rough, spherical particle with significant porosity. At 300 °C they are completely collapsed, leaving behind a porous solid residue.

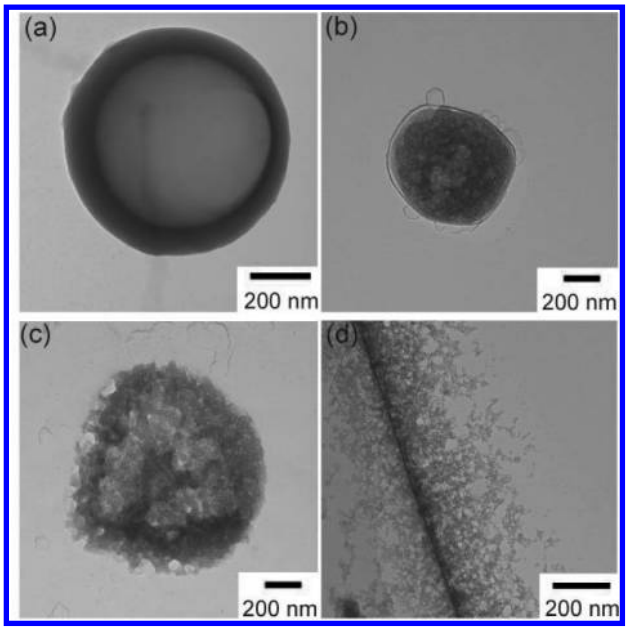

Figure 9. Effect of heating on toluene-plasma particles. TEM of the particles after heating at (a) 100 °C, (b) 200 °C, (c) 250 °C, and (d) 300 °C.

DISCUSSION

The decomposition of hydrocarbon molecules in the plasma is often described as a polymerization process. Although the product is not a true polymer with a repeating monomeric unit, it is a solid of cross-linked amorphous hydrogenated carbon.[50] Typically the final material is solid, but liquid-like products, sometimes referred to as oils, are also known to form under conditions that promote a low degree of cross-linking. Generally, low pressure and high power promote the formation of solid products, whereas low power and high pressure produce materials with a low degree of cross-linking that appear as oily films[47,48,51] or, as our results suggest, as micrometer-size droplets. In the experiments shown here, the plasma is operated at 400 mTorr and RF power of 5 W. Under these conditions, we expect the formation of oily materials. To confirm this hypothesis, we repeated the experiments at 200 mTorr and 20 W of RF power. Figure 7c shows particles collected after 5 min of operation of the plasma. They are very small (less than 100 nm in diameter), have a solid appearance, and remain unchanged under TEM. Their FTIR spectrum shows the same bands at 2860 and 2930 cm^{-1} as solid bubbles that are formed after exposing the plasma particles to TEM. This

dx.doi.org/10.1021/jp303793u | J. Phys. Chem. B 2012, 116, 11737−11743

confirms the presence of alkyl CH stretch (Figure 7c) and the absence of the aromatic group.

The elemental analysis of the plasma particles is given in Table 1. Three samples were analyzed: oily particles produced at low power (before exposure to TEM), microbubbles produced by exposing oily particles to TEM, and solid particles obtained at high power. The hydrogen−carbon ratio in all samples is less that in toluene (1.14). The solid particles and the microbubbles have very similar ratios, whereas oily particles before exposure to the beam have approximately 5% more hydrogen.

Table 1. Carbon−Hydrogen Ratios of Plasma Polymerized Toluene

sample	H/C ratio
toluene PP (oily) before exposure to e-beam	1.01
toluene PP after exposure to e-beam	0.95
toluene PP (solid)	0.95

In view of these results, the formation of microbubbles can be explained by the following scheme, in which liquid-like droplets with a low degree of cross-linking are converted into a solid material with higher degree of cross-linking while releasing hydrogen

$$\text{oily droplets} + \text{energy} \rightarrow \text{solid bubbles} + H_2$$

The bond dissociation energy of carbon bonds in plasma polymerized toluene is less than 7 eV (e.g., bond dissociation energy of C−C, C═C, and C−H is 3.61, 6.35, and 4.30 eV, respectively[50]). Given that the incident energy of the electron beam is 120 keV[52] and that the kinetic energy transferred to solids by the irradiation of the TEM beam is approximately 30 keV,[53] breaking carbon bonding is indeed feasible. It appears, therefore, that the formation of microbubbles is due to the further polymerization of partially cross-linked oily droplets with the simultaneous release of hydrogen, which explains the inflation of the bubble in TEM.

Electron beam irradiation in TEM has been reported previously to induce structural transformations in inorganic systems such as gold and platinum,[54] to produce metal nanostructures from Ag, Ni, Cr, Al, and Au.[55] In these processes, the electron serves as the external driving force by losing a portion of its kinetic energy due to inelastic interaction with materials. Besides TEM, high-resolution scanning electron microscopy (HRSEM)[53] has also been used for producing nanorods and nanoparticles.[53] In one particular study, it was shown that gold structure changes due to exposure to the electron beam in TEM and dynamically changes the shape of the crystal and causes it grow.[56] Amorphous iron oxide, Fe_2O_3, nanoparticles were shown to evolve to larger particles, while they were exposed to the electron beam and formed a hollow structure.[26] Similar evolution was observed for NaYF4:Yb,Er nanoparticles in TEM because of the interaction with the electron beam.[27] Although hollow polymeric particles have not been fabricated using an electron beam, this method has been applied to induce cross-linking for modification of polymers (e.g., polyphenylene) to improve their shape, wear, and mechanical properties.[57−60]

Formation of hollow nanoparticles by plasma polymerization was reported previously from a variety of organic precursors.[16] That process was also explained as a liquid-to-solid conversion, but the hollow nanoparticles were formed inside the plasma, not under subsequent treatment, and the void fraction was much smaller, less than 4%. The unusual feature of the present process is the inflation of spherical particles into microbubbles with a large volume fraction of about 90%. Given the proposed scheme for the formation of these structures, we may write an expression to relate the size of the initial liquid droplet to that of the final bubble

$$\frac{4\pi R_1^3}{3}\rho_1 = (4\pi R_2^2 h)\rho_2 + \delta m \quad (1)$$

where R_1 is the radius of the oily droplet; ρ_1 is its density; R_2 is the radius of the final bubble; h is the thickness of the shell; ρ_2 is the density of the cross-linked solid; and δm is the mass of hydrogen that is produced during cross-linking. From Table 1 we estimate the mass of released hydrogen to be 0.5% of the mass of the liquid particle. The relationship between R_1 and R_2 then becomes

$$R_1 = \left(\frac{3h\rho_2}{0.995\rho_1}\right)^{1/3} R_2^{2/3} \quad (2)$$

which implies a straight line between R_1 and $R_2^{2/3}$. This relationship is plotted in Figure 10 based on the experimental data. Indeed, the data show a linear relationship with zero intercept, as predicted from eq 2, with a slope of 0.603 $nm^{1/3}$. The thickness of the shell is 47 nm, and the density of the liquid particles is not known; however, we may approximate it with the density of liquid toluene, 0.86 g/cm^3. Using these values, we use the slope of the line in Figure 10 to estimate the density of the solid particle, which we find to be ρ_2 = 1.25 g/cm^3. Reported values for the density of plasma polymers are in the range of 1−1.5 g/cm^3.[61,62] The value calculated from the experimental data falls in the middle of this range, and this agreement lends further support to the mechanism of liquid-to-solid conversion that was used to interpret the formation of these bubbles.

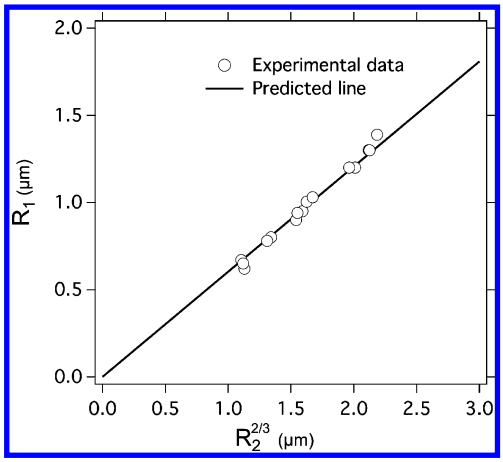

Figure 10. Relationship between particle radius before (R_1) and after (R_2) irradiation by a TEM beam. Experimental measurements are shown with open circles, and the solid line is calculated from eq 2 with ρ_2 = 1.25 g/cm^3.

CONCLUSIONS

We have demonstrated a one-step process for formation of hollow particles from plasma polymerized particles. In this process, the plasma produces a partially polymerized liquid

dx.doi.org/10.1021/jp303793u | J. Phys. Chem. B 2012, 116, 11737−11743

whose subsequent polymerization leads to the formation of a solid, the release of hydrogen, and the transformation of the liquid droplet into a microbubble with thin solid walls and high void fraction. This transformation was documented in detail using toluene as the precursor and was also observed with heptane. The formation of liquid droplets by plasma polymerization is reproducible provided that the plasma is operated under low power and high pressure. The transformation of these liquids into microbubbles is induced by various forms of energy, including electron beam, laser irradiation, and heating. This suggests that oily microdroplets by plasma polymerization may be engineered to serve as stimuli-responsive materials.

■ ASSOCIATED CONTENT

Supporting Information

Video recording the generation of the toluene microbubble using a transmission electron microscope. Particle is irradiated with a high-energy electron beam working at 120 keV. This material is available free of charge via the Internet at http://pubs.acs.org.

■ AUTHOR INFORMATION

Corresponding Author

*E-mail: matsoukas@engr.psu.edu. Phone: 814-863-2002. Fax: 814-865-7846.

Notes

The authors declare no competing financial interest.

■ ACKNOWLEDGMENTS

This research was supported in part by the National Science Foundation (CBET-0651283) and Advance Cooling Technology (117041PO9621). We also thank the nanofabrication facility at Penn State, Mengqian Li, and Erik Hsiao for helpful discussions.

■ REFERENCES

(1) Bertling, J.; Blömer, J.; Kümmel, R. *Chem. Eng. Technol.* **2004**, *27*, 829−837.
(2) Friedl, O.; Motz, C.; Peterlik, H.; Puchegger, S.; Reger, N.; Pippan, R. *Metall. Mater. Trans. B* **2008**, *39*, 135−146.
(3) Smith, B.; Szyniszewski, S.; Hajjar, J.; Schafer, B.; Arwade, S. *J. Constr. Steel Res.* **2011**, 1−10.
(4) Borodina, T.; Markvicheva, E.; Kunizhev, S.; Möhwald, H.; Sukhorukov, G. B.; Kreft, O. *Macromol. Rapid Commun.* **2007**, *28*, 1894−1899.
(5) Chen, J.-F.; Ding, H.-M.; Wang, J.-X.; Shao, L. *Biomaterials* **2004**, *25*, 723−727.
(6) Caruso, F.; Trau, D.; Möhwald, H.; Renneberg, R. *Langmuir* **2000**, *16*, 1485−1488.
(7) Guo, X.; Szoka, F. C. *Acc. Chem. Res.* **2003**, *36*, 335−341.
(8) Deng, J.; Yu, Y.; Dun, S.; Yang, W. *J. Phys. Chem. B* **2010**, *114*, 2593−2601.
(9) Cao, X.; Gu, L.; Zhuge, L.; Gao, W.; Wang, W.; Wu, S. *Adv. Funct. Mater.* **2006**, *16*, 896−902.
(10) Su, J.; Ren, L.; Wang, L. *Colloid Polym. Sci.* **2005**, *284*, 224−228.
(11) Rennel, C.; Rigdahl, M. *Colloid Polym. Sci.* **1994**, *272*, 1111−1117.
(12) Gane, P. A.; Kettle, J. P.; Matthews, G. P.; Ridgway, C. J. *Ind. Eng. Chem. Res.* **1996**, *35*, 1753−1764.
(13) Lou, X. W. D.; Archer, L. A.; Yang, Z. *Adv. Mater.* **2008**, *20*, 3987−4019.
(14) Messing, G. L.; Zhang, S.-C.; Jayanthi, G. V. *J. Am. Ceram. Soc.* **1993**, *76*, 2707−2726.
(15) Jokanović, V.; Spasić, A. M.; Uskoković, D. *J. Colloid Interface Sci.* **2004**, *278*, 342−352.
(16) Cao, J.; Matsoukas, T. *J. Nanopart. Res.* **2004**, *6*, 447−455.
(17) Liu, J. G.; Wilcox, D. L. *J. Mater. Res.* **1995**, *10*, 84−94.
(18) Wan, S.; Guo, F.; Shi, L.; Peng, Y.; Liu, X.; Zhang, Y.; Qian, Y. *J. Mater. Chem.* **2004**, *14*, 2489−2491.
(19) Heiskanen, H.; Denifl, P.; Hurme, M.; Pitkänen, P. *Chem. Eng. Technol.* **2010**, *33*, 682−691.
(20) Zeng, H. C. *Curr. Nanosci.* **2007**, *3*, 177−181.
(21) Voorhees, P. W. *J. Stat. Phys.* **1985**, *38*, 231−252.
(22) Zrínyi, M. *Colloids Surf., A* **2011**, *382*, 192−197.
(23) Hosoda, H.; Takeuchi, S.; Inamura, T.; Wakashima, K. *Sci. Technol. Adv. Mater.* **2004**, *5*, 503−509.
(24) Lee, E.; Kim, B. *Korean J. Chem. Eng.* **2011**, *28*, 1347−1350.
(25) Yan, Z.; Bao, R.; Huang, Y.; Chrisey, D. B. *J. Phys. Chem. C* **2010**, *114*, 11370−11374.
(26) Latham, A. H.; Wilson, M. J.; Schiffer, P.; Williams, M. E. *J. Am. Chem. Soc.* **2006**, *128*, 12632−12633.
(27) Sun, W. F. L.-D.; Zhang, Y.-W.; Yan, C.-H. *Small* **2009**, *5*, 2057−2060.
(28) Xu, X.; Asher, S. A. *J. Am. Chem. Soc.* **2004**, *126*, 7940−7945.
(29) Yan, S.; Maeda, H.; Hayashi, J. I.; Kusakabe, K.; Morooka, S.; Okubo, T. *J. Mater. Sci.* **1993**, *28*, 1829−1833.
(30) Shahravan, A.; Matsoukas, T. *J. Nanopart. Res.* **2012**, *14*, 1−11.
(31) Goodman, J. *J. Polym. Sci.* **1960**, *44*, 551−552.
(32) Biederman, H.; SlavInska, D. *Surf. Coat. Technol.* **2000**, *125*, 371−376.
(33) Massereau-Guilbaud, V.; Pereira, J.; Geraud-Grenier, I.; Plain, A. *J. Appl. Phys.* **2009**, *105*, 033302−8.
(34) Abbasi, F.; Mirzadeh, H.; Katbab, A.-A. *Polym. Int.* **2001**, *50*, 1279−1287.
(35) Shi, F. F. *Surf. Coat. Technol.* **1996**, *82*, 1−15.
(36) Yasuda, H. K. *Plasma Processes Polym.* **2005**, *2*, 293−304.
(37) Cao, J.; Matsoukas, T. *J. Appl. Phys.* **2002**, *92*, 2916−2922.
(38) Ho, C.-P.; Yasuda, H. *J. Appl. Polym. Sci.* **1990**, *39*, 1541−1552.
(39) Cho, S.-G.; Ko, K.-C. *Thin Solid Films* **2010**, *518*, 6619−6623.
(40) Grill, A. *Dielectric Films for Advanced Microelectronics*; John Wiley & Sons, Ltd.: New York, 2007; pp 1−32.
(41) Li, D.; Vrtis, R.; Shahravan, A.; Matsoukas, T. *J. Nanopart. Res.* **2011**, *13*, 985−996.
(42) Pocsik, I.; Veres, M.; Fule, M.; Koos, M.; Kokavecz, J.; Z. Toth, G. R. *Vacuum* **2003**, *71*, 171−176.
(43) Pereira, J.; Geraud-Grenier, I.; Massereau-Guilbaud, V.; Plain, A. *Thin Solid Films* **2005**, *482*, 226−231.
(44) Stoykov, S.; Eggs, C.; Kortshagen, U. *J. Phys. D: Appl. Phys.* **2001**, *34*, 2160−2173.
(45) Zielinski, T.; Kijenski, J. *Composites, Part A: Appl. Sci. Manufacturing* **2005**, *36*, 467−471.
(46) Tavares, J.; Coulombe, S. *Powder Technol.* **2011**, *210*, 132−142.
(47) Qin, C.; Coulombe, S. *Plasma Sources Sci. Technol.* **2007**, *16*, 240−249.
(48) Bölük, M. Y.; Akovali, G. *Polym. Eng. Sci.* **1981**, *21*, 664−667.
(49) Fujii, A.; Fujimaki, E.; Ebata, T.; Mikami, N. *J. Chem. Phys.* **2000**, *112*, 6275−6284.
(50) Yasuda, H. *Plasma Polym.* **1985**.
(51) Kobayashi, H.; Bell, A. T.; Shen, M. *Macromolecules* **1974**, *7*, 277−283.
(52) Williams, D. B.; Carter, C. B. *Transmission electron microscopy: a textbook for materials science*; Springer: New York, 2009.
(53) Chen, K. H.; Wu, C. T.; Hwang, J. S.; Wen, C. Y.; Chen, L. C.; Wang, C. T.; Ma, K. J. *J. Phys. Chem. Solids* **2001**, *62*, 1561−1565.
(54) Zandbergen, H. W.; van Duuren, R. J. H. A.; Alkemade, P. F. A.; Lientschnig, G.; Vasquez, O.; Dekker, C.; Tichelaar, F. D. *Nano Lett.* **2005**, *5*, 549−553.
(55) Fischbein, M. D.; Drndić, M. *Nano Lett.* **2007**, *7*, 1329−1337.
(56) Bovin, J. O.; Wallenberg, R.; Smith, D. J. *Nature* **1985**, *317*, 47−49.
(57) Qi, X.; Huang, Y.; Klapper, M.; Boey, F.; Huang, W.; Feyter, S. D.; Müllen, K.; Zhang, H. *J. Phys. Chem. C* **2010**, *114*, 13465−13470.
(58) Muratoglu, O. K.; Bragdon, C. R.; O'Connor, D. O.; Jasty, M.; Harris, W. H. *J. Arthroplasty* **2001**, *16*, 149−160.

(59) Dijkstra, D. J.; Pennings, A. J. *Polym. Bull.* **1987**, *17*, 507−513.
(60) Christman, K. L.; Schopf, E.; Broyer, R. M.; Li, R. C.; Chen, Y.; Maynard, H. D. *J. Am. Chem. Soc.* **2009**, *131*, 521−527.
(61) Choukourov, A.; Gordeev, I.; Arzhakov, D.; Artemenko, A.; Kousal, J.; Kylián, O.; Slavínská, D.; Biederman, H. *Plasma Processes Polym.* **2012**, *9*, 48−58.
(62) Rau, C.; Kulisch, W. *Thin Solid Films* **1994**, *249*, 28−37.